Preneoplastic lesion growth driven by the death of adjacent normal stem cells

Dennis L. Chao*†, J. Thomas Eck‡, Douglas E. Brash§, Carlo C. Maley¶, and E. Georg Luebeck‖

*Vaccine and Infectious Disease Institute and ‖Program in Computational Biology, Fred Hutchinson Cancer Research Center, Seattle, WA 98109; ‡BioMaPS Institute for Quantitative Biology, Rutgers University, New Brunswick, NJ 08901; §Departments of Therapeutic Radiology, Genetics, and Dermatology and Yale Comprehensive Cancer Center, Yale School of Medicine, New Haven, CT 06520; and ¶Molecular and Cellular Oncogenesis Program, Wistar Institute, Philadelphia, PA 19104

Edited by Stanley M. Gartler, University of Washington, Seattle, WA, and approved July 24, 2008 (received for review March 6, 2008)

Clonal expansion of premalignant lesions is an important step in the progression to cancer. This process is commonly considered to be a consequence of sustaining a proliferative mutation. Here, we investigate whether the growth trajectory of clones can be better described by a model in which clone growth does not depend on a proliferative advantage. We developed a simple computer model of clonal expansion in an epithelium in which mutant clones can only colonize space left unoccupied by the death of adjacent normal stem cells. In this model, competition for space occurs along the frontier between mutant and normal territories, and both the shapes and the growth rates of lesions are governed by the differences between mutant and normal cells' replication or apoptosis rates. The behavior of this model of clonal expansion along a mutant clone's frontier, when apoptosis of both normal and mutant cells is included, matches the growth of UVB-induced *p53*-mutant clones in mouse dorsal epidermis better than a standard exponential growth model that does not include tissue architecture. The model predicts precancer cell mutation and death rates that agree with biological observations. These results support the hypothesis that clonal expansion of premalignant lesions can be driven by agents, such as ionizing or nonionizing radiation, that cause cell killing but do not directly stimulate cell replication.

clonal expansion | computer simulation | skin cancer | TP53 | UVB

The expansion of premalignant lesions is an important step in the progression to cancer, because it greatly increases the probability that they can acquire additional mutations. Large premalignant clones have been found in normal skin (1, 2), head and neck (3), lung (4), bladder (5), and esophagus (6). One mechanism by which clones could expand is the acquisition of a mutation that increases cell proliferation. However, many factors affect tumor evolution (7). An alternative is the opportunistic colonization of space left vacant by the death of neighboring cells, whether by normal cell loss or by cytotoxic exposures such as radiation and oxidative stress that produce free radicals. Therefore, the growth of a mutant clone's territory can be driven by the death of adjacent normal cells without additional mutations (8–10).

The classic keratinocyte territory is the epithelial proliferative unit (EPU), a group of 10–14 nucleated keratinocytes that includes a single long-lived stem cell, nine transit-amplifying (TA) cells, which undergo several divisions before becoming postmitotic (PM), and several suprabasal PM cells squaming upward (11). Recently, evidence supporting an alternative hypothesis of a "committed progenitor" (CP) cell, in which stem and TA roles are combined in an immortal CP cell, emerged in a study involving single-cell labeling of mouse tail keratinocytes (12). In this new model, dividing CPs usually generate one CP and one PM, but they can also produce two CPs or two PMs (12, 13). The proportion and rates of these events set a characteristic territory size of 3.5 PMs per CP in the tail skin (14). However, CP lineages occasionally expand beyond this size over the course of months, whenever the rare CPs that generate two CP daughters replace those that generated two short-lived PMs. In back skin, the tissue used in the present study, the same technique showed clusters of 10 labeled basal cells that remained stable for 6 months despite 30–50% growth in skin area. Whether this result, which is consistent with EPU sizes, indicates that back-skin-tissue architecture differs from tail or demonstrates that the CP population can form large stable CP domains is considered in *Discussion*. Regardless of whether skin is organized into EPUs or CPs and PMs, neither territory has physical walls, so growth restraint comes from neighboring cells. Both kinds of territory can expand only at their frontiers.

UVB causes characteristic *p53* mutations in keratinocytes. Because *p53* mutations lead to p53 protein overstabilization, mutant cells can be stained with anti-p53 antibodies and the mutation confirmed by DNA sequencing. It is believed that, in the absence of other influences, a *p53*-mutant progenitor cell and its progeny are confined to their EPU (9). Yet chronic UVB exposure generates, within 3–5 weeks, clones of *p53*-mutant keratinocytes several times larger than a putative EPU or territory of CPs undergoing spontaneous expansion in tail skin.

These are clones of a single progenitor, because the same mutation is present throughout the lesion and because UV mutation frequencies are too low ($\approx 10^{-4}$ per gene per cell generation) to create multiple adjacent mutant clones. Chronic UVB exposure evidently establishes rapid territory-escape events that overwhelm the normal proliferative steady-state. Cells with inactivated *p53* are resistant to UVB-induced apoptosis and, thus, have a survival advantage over normal cells in skin subjected to UVB exposure (9, 15, 16). *p53*-mutant clones have been found to be larger and more frequent in chronically sun-exposed skin in humans (1). These cells are the putative precursors to squamous cell carcinoma (15, 17, 18), and therefore, their expansion may lead to an increased risk of developing cancer.

Lesion growth is conventionally assumed to be linked to elevated cell proliferation and so is frequently modeled without reference to tissue architecture, but this assumption is most appropriate for cells with no spatial constraints, such as hematologic malignancies or cultured cells inoculated as xenografts. Here, we explore the dynamics of premalignant lesion growth in a spatially structured tissue by using a simple computational model, which we call the frontier model. In this model, progenitor cells are situated on a 2D hexagonal lattice and die at a low rate that is elevated by physical or chemical agents. The hexagonal lattice can represent the hexagonal geometry of EPUs, which are outlined by a single flattened and keratinized superficial cell, or any other closely packed proliferative units, such as

Author contributions: D.L.C., J.T.E., D.E.B., C.C.M., and E.G.L. designed research; D.L.C. and D.E.B. performed research; D.L.C. and J.T.E. contributed new reagents/analytic tools; D.L.C. and E.G.L. analyzed data; and D.L.C., D.E.B., C.C.M., and E.G.L. wrote the paper.

The authors declare no conflict of interest.

This article is a PNAS Direct Submission.

†To whom correspondence should be addressed. E-mail: dchao@fhcrc.org.

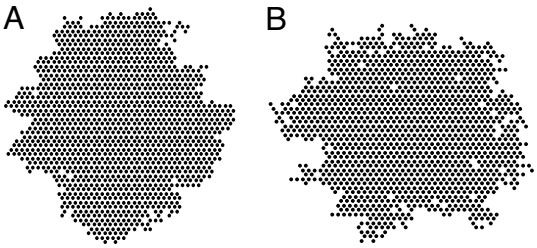

Fig. 1. Images of simulated clones. (*A*) Ten-year-old survival mutant clone ($k_{reproductive} = 1$, $k_{survival} = 0$) occupying 1,435 sites. (*B*) Three-year-old reproductive mutant clone ($k_{reproductive} = 10$, $k_{survival} = 0$) with 1,361 sites. Reproductive mutant clones have longer and more irregular perimeters.

CP territories or intestinal crypts. When a territory's progenitor cell dies, its living neighbors compete to occupy its site and thereby clonally expand. If a mutant is even partially resistant to apoptosis, it is likely to expand over time. Clonal expansion is important at several stages in cancer progression (16), but at the early stage modeled here, the spreading events are confined to the basal cell layer without confounding upward or downward ectopic proliferation (1). We compare the model-generated simulations of lesion numbers and sizes to corresponding *p53*-mutant lesions observed in the skin of mice exposed to UVB. The frontier model matches the observed growth of precancerous lesions across mouse epidermis, whereas a standard exponential growth model, which makes no reference to tissue architecture, does not.

Results

Simulated 2D Lesion Growth Is Quadratic. We defined the territory, or area, of a simulated mutant clone, N, to be the number of mutant sites derived from a single progenitor. We defined the perimeter of a clone to be the sites, which can be either empty or occupied by progenitor cells, that are adjacent to any of the clone's cells, and P to be the number of sites in the perimeter. For a mutant clone to grow, it must colonize empty sites in its perimeter. Mutant cells have an apoptosis rate that is $k_{survival}$ times that of normal and the ability to colonize an adjacent empty site at $k_{reproductive}$ times a normal cell's rate.

We compared the clonal growth rates of two types of simulated mutants, a reproductive mutant and a survival mutant. The reproductive mutant's progenitor cells could proliferate in response to the death of a neighboring cell 10 times faster than a normal cell ($k_{reproductive} = 10$), whereas the survival mutant's replication rate was the same as normal ($k_{reproductive} = 1$). These two cell types represent extreme behavior, allowing us to see how sensitive the model's behavior is to large differences in replication rates between mutant and normal cells. Both mutants had no cell death ($k_{survival} = 0$), so that territory colonized by a mutant remained mutant. We also simulated the behavior of a reproductive mutant that had the same death rate as normal cells ($k_{reproductive} = 10$, $k_{survival} = 1$) and found that although these mutants often went extinct, the clones that survived had growth rates similar to the reproductive mutant with no cell death (data not shown). Simulations were initialized with a single mutant EPU in the middle of a tissue consisting of 400×400 progenitor cells, large enough so that the boundaries of the tissue did not impede the growth of the mutant clone. For normal cells, the mean time it took for a stem cell to divide symmetrically to colonize an empty site, r, was set to 1 day and the death rate, λ, to 0.01 day^{-1} (3.65 year^{-1}). Representative simulated mutant clones are shown in Fig. 1.

Because a clone in the frontier model can expand only by colonizing its perimeter (P), we can also express the rate of clone area growth (dN/dt) in terms of two constants and its perimeter size:

$$\frac{dN}{dt} = \lambda \times \Pr\{\text{a site will be colonized by a mutant}\} \times P(t). \quad [1]$$

λ is the death rate of normal progenitor cells in the perimeter of a mutant clone. The second term represents the mutant's ability to colonize available empty sites and can be determined by the shape of the clone and its reproductive advantage ($k_{reproductive}$). The probability that an empty site will be colonized by a mutant depends on the numbers of its mutant and normal neighbors; a site with many mutant neighbors is more likely to be colonized by a mutant than a site with fewer mutant neighbors. We calculated that a reproductive mutant colonizes an empty site in its perimeter an average of 83% of the time, and a survival mutant could 37% of the time (Table 1). We found these probabilities to be stable during the growth of lesions (data not shown).

The final term in eq. 1 is the clone's perimeter size, $P(t)$. We observed that in the frontier model, the perimeter grew linearly

Table 1. The probability that an empty site (depicted by the gray hexagons) will be colonized by a mutant (hexagons with Ms)

							
Survival mutant							
Fraction of sites*	0.38	0.28	0.18	0.10	0.05	0.02	
Colonization probability	×17%	×33%	×50%	×67%	×83%	×100%	
	6.3%	+ 9.2%	+ 9.1%	+ 6.4%	+ 4.0%	+ 2.1%	**= 37.0%**
Reproductive mutant							
Fraction of sites†	0.33	0.22	0.16	0.12	0.10	0.09	
Colonization probability	×67%	×83%	×91%	×95%	×98%	×100%	
	21.7%	+ 18.2%	+ 14.3%	+ 11.0%	+ 9.6%	+ 8.5%	**= 83.3%**

The fractions of normal sites in survival and reproductive mutant clone perimeters with one to six mutant neighbors were counted. The probability that these sites will be colonized by a mutant was computed in *Methods*. The inner product of these two vectors, shown in bold on the right, is the average probability that a site in a clone's perimeter will be colonized by the mutant.

*Average fraction (over 10 simulations) of sites with 1. . . 6 mutant neighbors in the perimeter of a survival mutant clone ($k_{reproductive} = 1$, $k_{survival} = 0$) after 25 simulated years.

†Average fraction of sites (over 10 simulations) with 1. . . 6 mutant neighbors in the perimeter of a survival mutant clone ($k_{reproductive} = 10$, $k_{survival} = 0$) after 10 simulated years.

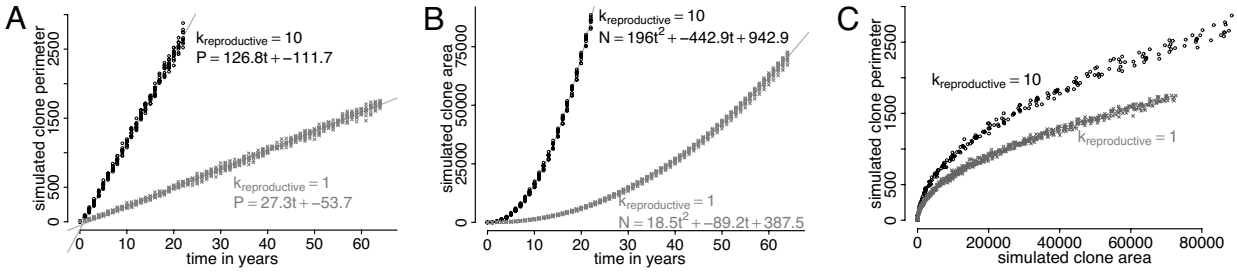

Fig. 2. Perimeter and area growth of mutant clones with reproductive and survival advantages or just a survival advantage alone. For all three plots, the data from 10 runs of a mutant with reproductive and survival advantages ($k_{reproductive} = 10$ and $k_{survival} = 0$) and from 10 runs of a mutant with only a survival advantage ($k_{reproductive} = 1$ and $k_{survival} = 0$) are shown. (*A*) Perimeter vs. clone area. (*B*) Perimeter vs. time. Lines indicate linear regression fits, which exclude data from the first 5 years. (*C*) Clone area vs. time. The lines are the fits to $n = at^2 + bt + c$, which exclude data from the first 5 simulated years.

over time [$P(t) = 126.8t - 111.7$ for the reproductive mutant and $27.3t - 53.7$ for the survival mutant] (see Fig. 2*A*). Because the rate of clone area growth (dN/dt) grows linearly over time, clone area (N) growth is quadratic, i.e., a function of time squared. Applying eq. 1 to predict the growth rate of the reproductive mutant ($k_{reproductive} = 10$, $k_{survival} = 0$):

$$\frac{dN}{dt} = 3.65 \times 83\% \times (126.8t - 111.7) \quad [2]$$

$$N = 192.1t^2 - 338.4t + c, \quad [3]$$

where c is an integration constant. This result agrees well with the least-squares quadratic fit to the simulated clone area data (Fig. 2*B*): $n = 196.0t^2 - 442.9t + 942.9$. The survival mutant's growth can be predicted in the same manner to find that $n = 18.4t^2 - 7\,2.5t + c$, which also agrees with the simulation data: $n = 18.5t^2 - 89.2t + 387.5$. This agreement shows that (*i*) growth of mutant clones in a 2D epithelium is likely to be quadratic rather than exponential and (*ii*) eq. 1 is sufficient to predict lesion growth rates.

The reproductive mutant's clones had longer perimeters than the survival mutant's for clones of the same size (Fig. 2*C*). The longer perimeters reflect the larger protrusions and roughness of the clones' edges (Fig. 1). A clone with a reproductive advantage grew faster, because it had both a longer perimeter (Fig. 2*C*) and a temporal advantage in colonizing adjacent empty space (Table 1). In the simulations, a mutant that replicated 10 times faster had a perimeter that grew $126.8/27.3 = 4.6$ times faster and was $83\%/37\% = 2.2$ times more likely to colonize an empty site in its perimeter than a similarly death-resistant mutant clone that colonized empty space at the same speed as normal cells.

Estimating Growth Parameters of Experimental Mouse Skin Lesions. We compared *p53*-mutant lesion size data in mice (9) to two different model scenarios: (*i*) *p53*-mutant lesions grow exponentially and (*ii*) *p53*-mutant lesions grow according to the frontier model described above. To determine whether the model-generated data were consistent with the empirical data, we used a two-sample Smirnov test for comparing discrete distributions (19). A low P value indicates that the model was not consistent with the empirical observations. We also used quantile-quantile (Q-Q) plots to compare graphically the distributions of model-generated clone sizes with those measured in mouse skin (Fig. 3). A Q-Q plot is a sensitive graphical method to detect differences between two empirical distributions (20). Q-Q plots compare two distributions by plotting the values of the distributions at various percentiles. Identical distributions would result in a Q-Q plot that falls along the diagonal (indicated in the plots).

Most tumor models assume that all cells in the lesion replicate at a fixed rate in the absence of resource limitations, resulting in exponential growth. With a growth rate of 0.33 week^{-1} (clone sizes double every 2.1 weeks), the exponential model generated clone sizes consistent with the mouse lesion-size distribution at both weeks 8 and 10 ($P = 0.16$ and $P = 0.96$), but the Q-Q plot revealed that the model underestimated clone sizes at week 8 (Fig. 3*A*). With a growth rate of 0.36 week^{-1} (clones double every 1.9 weeks), there was better statistical agreement with the empirical data at week 8 ($P = 0.52$ and $P = 0.60$ for weeks 8 and 10), but the Q-Q plot revealed that the exponential model overestimated the sizes of the largest clones at both weeks 8 and 10 (Fig. 3*B*). Although the exponential model can produce data that is broadly consistent with the empirical measurements, the systematic deviations from the empirical data visible in the Q-Q plots indicate that exponential growth may be too fast to account for skin-lesion growth.

We next compared the mouse lesion data to the output from the frontier model in which *p53*-mutant cells are either (*i*)

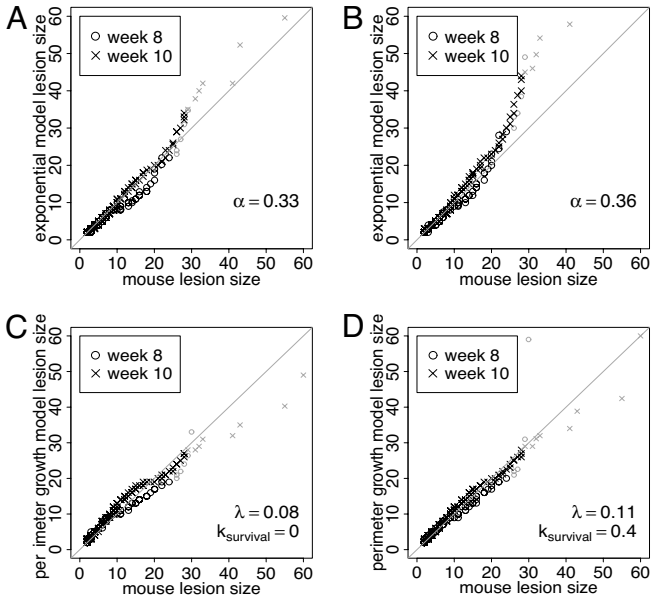

Fig. 3. Q-Q plots comparing actual and simulated clone sizes. Shown are Q-Q plots comparing the mouse data with an exponential clonal expansion model having a growth rate of 0.33 week^{-1} (*A*) and 0.36 week^{-1} (*B*). The top 5th percentile of clone sizes are plotted in gray. Comparisons of the mouse data with the frontier growth model with no mutant death ($k_{survival} = 0$, $\lambda = 0.08$) (*C*) and with mutant death ($k_{survival} = 0.4$, $\lambda = 0.11$) (*D*). *p53*-mutant clone sizes are estimates of the number of mutant EPUs in mouse epidermis, and clones of less than 16 cells were excluded. Likewise, simulated clones smaller than two EPUs were excluded in the comparisons.

Table 2. Simulation parameters that match the mouse lesion data, corresponding to Fig. 3*D* and values obtained from the literature

	Model	Literature
Parameters derived from literature		
$k_{reproductive}$	1.0	1.0*
$k_{survival}$	0.4	0.4†
r (day^{-1})	1.0	ND‡
Parameters derived from simulations		
λ (day^{-1})	0.11	0.12
μ (mut per EPU per day)	7.7×10^{-6}	12.5×10^{-6}

*We found no evidence that *p53*-mutant keratinocytes can colonize adjacent space faster than normal cells.

†*p53*-mutant cells undergo UVB-induced apoptosis at 40% of the rate of normal cells (15).

‡We did not find estimates in the literature for the time it takes for an EPU to colonize an adjacent empty space.

immortal ($k_{survival} = 0$) or (*ii*) partially resistant to UVB, with their rate of apoptosis being 40% of that of normal cells ($k_{survival} = 0.4$) as measured in ref. 15. For each simulation run, a single mutant progenitor cell was seeded in the middle of the tissue at a (uniform) random time during one simulated year to mimic the process of a *p53*-mutant EPU arising during continuous exposure to UVB. The mean symmetric division time in response to neighboring cell apoptosis was set to 1 day. The model was run 5,000 times each for different values of the wild-type death rate λ to simulate the growth of 5,000 different mutants that arise during one year. Larger values of λ resulted in a greater proportion of large lesions because of faster mutant expansion (16). The simulations with no *p53*-mutant death did not produce data consistent with the mouse data at both weeks 8 and 10 (e.g., $P = 0.04$ and $P = 0.10$ for weeks 8 and 10 when $\lambda = 0.08$) (Fig. 3*C*). Adding a realistic *p53*-mutant apoptosis rate improved the match to the experimental data. With $k_{survival} = 0.4$ and $\lambda = 0.11$, the frontier model was consistent with the mouse data ($P = 0.33$ and $P = 0.54$ for weeks 8 and 10), and there were no visible systematic deviations from the empirical data at either time point (Fig. 3*D*).

The remaining free parameter in the frontier model is the EPU mutation rate, which can also be derived from the mouse lesion data and which affects the total number of mutants generated during a simulation but not their clone size distribution. At week 10, the mouse skin had 151 clones of more than 16 cells (i.e., larger than one EPU) in an area of 4.46 cm^2, or an average of 33.84 clones per cm^2. With an estimated 1,400 EPUs per mm^2 of skin (11), there were $151/4.46/140000 = 2.42 \times 10^{-4}$ clones per EPU at week 10. For the model with *p53*-mutant death and $\lambda = 0.11$, a mutation rate of 7.7×10^{-6} mutations per EPU per day would generate this number of mutant clones per EPU. Table 2 summarizes the frontier model parameters that best fit the mouse data and measurements from the literature.

Discussion

Quadratic vs. Exponential Growth. The frontier model of opportunistic clonal expansion is more consistent with skin-lesion growth than exponential growth uninhibited by spatial constraints. Tumor promotion may not require an intrinsic propensity toward clonal expansion but could be passive, induced by the killing of neighboring normal cells. This possibility also provides an explanation for tumor promotion predicted for ionizing radiation in lung cancer (21). Spatial constraints not only slow mutant growth, they enforce a qualitatively different growth law.

Lesions exhibited quadratic growth in the frontier model, because clones could only expand along their edges. This behavior is consistent with that of similar simulation-based models (22) in which an object's growth is restricted to its boundaries. When lesion expansion is driven by other mechanisms, the growth dynamics can be different. Lesion growth is exponential when all of its cells divide at a constant rate. However, exponential growth is unlikely to be sustained in larger lesions, which may be limited by lack of adequate vasculature (23). Gompertzian dynamics, which feature an initial exponential growth phase followed by saturation, may be a more appropriate model for such systems (24). Stem cells from the bulge region of hair follicles may be responsible for repair of more macroscopic epidermal wounds (25), which could result in dynamics different from those described in the present model, which assumes that stem-like cells of the interfollicular epidermis are responsible for skin maintenance (26, 27).

Brú *et al.* (28) observed that the diameters of both cancer-cell colonies *in vitro* and certain tumors *in vivo* grew linearly over time, which is consistent with our simulations. The authors postulated that growth occurs by diffusion of the cancer cells from the tumor boundary, whereas in the frontier model, tumor and normal cells compete for space on sites on a lattice. Although both frameworks result in linear growth, the choice of model should depend on the physical characteristics of the system studied so that the model parameters correspond to properties of the cells. The frontier model applies to tissues in which lesion growth is driven by opportunistic expansion, such as *p53*-inactivated clones in skin (9) and possibly early lesions in the colon, Barrett's esophagus, and lung.

The mechanism by which a mutant cell colonizes a stem-cell-less EPU in these tissues is unknown, but in the *Drosophila* germline stem-cell niche, an empty stem cell compartment can be repopulated by the migration of a nearby epithelial stem cell or by dedifferentiation of a TA cell (29, 30).

The frontier model can be applied to an epidermis composed of either EPUs or CPs. Cell division to compensate for apoptosis is an intrinsic feature of the model, in which the mechanism for homeostatic cell divisions is an explicit consequence of the spatial relationships between cells. Because the UVB-induced apoptosis rate in our mouse study was much higher than the spontaneous symmetric division rate of CPs estimated in ref. 12, apoptosis-driven division should dominate the dynamics no matter which model of intraterritory growth is applied to the mouse data. Because the frontier model involves neither the internal workings of the proliferative unit nor the exact mechanism of unit replication, we modeled the expansion of *p53*-mutant stem cells in mouse skin while omitting their terminally differentiated progeny from the model. We estimated the *p53*-mutant stem cell population of a clone to be the total number of *p53*-inactivated cells divided by the estimated number of cells per EPU in irradiated skin (16 cells). If back skin were composed of CPs and PMs rather than EPUs, we would divide the number of *p53*-mutant cells by 4.5 [one plus the number of PMs per CP in mouse tail (12)] instead of 16, and the clones would thus be 3.6 times larger than in the EPU model. However, the model would fit this rescaled data equally well; because growth is quadratic in the frontier model, scaling the normal cell apoptosis rate (λ) to be $\sqrt{3.6} = 1.9$-fold higher would produce clones that are 3.6 times larger.

One remaining issue when applying the CP model to mouse back skin is that the number of cells per back-skin domain appears to be constant while the mouse grows [see supplemental figure 3A in ref. 12]. How can CP proliferation dynamics produce a clonal domain of stable size in growing skin? Reduced rates of spontaneous CP and PM cell loss (governed by CP $\rightarrow$ two PM events and the migration of basal PMs to the suprabasal layer) would generate skin growth and the remaining CP $\rightarrow$ two CP and CP $\rightarrow$ CP + PM events would be difficult to distinguish from the standard EPU model with an immortal stem cell producing differentiated TA cells. Interestingly, the underlying mechanism

of *p53*-mutant clonal expansion may be different in a stochastic CP system compared with a tissue composed of EPUs. Apoptosis-resistant *p53* mutants will tend to survive after irradiation but must compete with surviving normal CP cells, so mutant clones will rarely expand significantly. What dramatically increases the success of *p53* mutants, and thus the frequent clonal expansion seen in mouse back skin in ref. 9, is most likely the *p53* mutant's resistance to UVB-induced cell-cycle delay. This delay will transiently inhibit the cell division of all *p53*-wildtype CP competitors after every irradiation, so that a *p53* mutant would prevail consistently over normal cells.

As noted in ref. 40, restricting tumor growth to its edges has a large impact on estimates of cell-proliferation rates based on observed lesion sizes. In the frontier model, clones with shorter replication times grew faster but not at rates proportional to their division rates, as would be assumed under exponential growth. A simulated clone's growth was proportional to the length of its perimeter and to the probability that it could successfully compete with normal cells for space. These parameters are determined by the normal cell-death rate and the mutant's survival and replicative advantages over normal cells.

Biological Plausibility of Model-Derived Parameter Estimates. The simple frontier model of opportunistic clonal expansion described here can be used to estimate mutation and apoptosis rates, as well as some properties of mutant cells. However, exploring parameter space is inefficient, because a large number of simulations must be run to obtain the distribution of outcomes for a given set of parameters. In our analysis of *p53*-mutant lesion data, we used estimates from the literature to restrict the parameters. Specifically, we used empirical estimates of the apoptosis resistance of *p53*-mutant keratinocytes under UVB exposure, and we found no evidence in the literature that they have a reproductive advantage over normal cells. Therefore, only one free parameter (the normal cell death rate, λ) affected the mutant-clone size distribution.

The model accommodates scenarios in which mutant clones proliferate faster in response to the apoptosis of neighbors than normal compartments, which not only increases the growth rate of the lesion but also affects the shape of the lesion. For lesions of a given size, we observed that mutants with higher high replication rates had longer boundaries. The boundary size or a related metric, such as roughness (28), could be measured in lesions, and a comparison with the model using different replication rate differentials could be used to estimate the compartment replication rate of the mutant.

Using the frontier model, we estimated that the stem-cell mutation rate in mouse skin exposed to UVB is 7.7×10^{-6} mutations per EPU per day (Table 2). In proliferating cells in culture, the mutation rate after UV radiation exposure is 10^{-4} per gene per cell division (31). If the mutation rate is 10^{-4} per cell division and a stem cell undergoes asymmetric division every eight days to produce an amplifying cell or PM (12, 32), then the stem cell mutation rate is $10^{-4}/8 = 1.25 \times 10^{-5}$ per gene per day, which is in good agreement with our estimate. The percentage of apoptotic cells at the UVB dose used in the mouse experiments (1,250 J/m^2, a minimal erythemal dose that induces a barely perceptible sunburn) was $\approx$1.5% in wild-type mice after 1 day of exposure (D. Knezevic and D.E.B., unpublished work; see also ref. 41). If an epidermal cell that is undergoing apoptosis is visible for 4 h (33–35), then the apoptosis rate is $0.02/4\ \text{h} = 0.12\ \text{day}^{-1}$, which agrees with the model's estimate of $0.11\ \text{day}^{-1}$. When we decreased the apoptosis rate of simulated *p53* mutants from 40% of a normal cell (the estimate from the literature) to an unrealistically low 0%, the model did not fit the empirical data. Thus, we have demonstrated that the frontier model can be used to quantitate precancerous lesion dynamics.

Materials and Methods

Tissue Simulation Model. We implemented a stochastic event-driven model of a tissue (Java source code, tested on Sun's Java Runtime Environment 1.6.0-06, is available on request from the corresponding author). The tissue is represented by a hexagonal lattice in which each point on the lattice represents a site that is either occupied (presumably by a single progenitor cell) or empty. Cell replication and deaths are scheduled in an event queue, and time progresses in the simulation by drawing events from the queue in chronological order.

The probability of a cell dying is constant over time, so for computational efficiency, the time of a cell's death is drawn from an exponential distribution $E(t;\lambda) = \lambda e^{-\lambda t}$ as soon as it is created. When the death event is drawn from the event queue, the cell's location on the lattice is emptied and any pending replication events scheduled for that site are canceled.

A death event triggers the cells adjacent to the newly empty site (up to six neighbors) to schedule division events, with division times drawn from an exponential distribution $E(t;r)$. When a cell divides, it copies itself into an adjacent empty site, although not necessarily the neighbor that had triggered the event. Thus, when a cell dies, the neighbor with the shortest time to division will fill it. However, the cells that do not win this competition are briefly ''primed'' to divide. When their division events occur, they can fill any adjacent empty site, even if the site that had triggered the event is already occupied. If a cell tries to divide when there is no available space, division does not occur. After division occurs, the parent and daughter schedule additional division events if there are adjacent empty sites.

Thus far, the model describes normal tissue, as might be seen in a healing burn wound. To simulate tumorigenesis, cells can be normal (wild-type) or mutant. Mutants can have two kinds of advantages over normal cells in this model. Mutants may be assigned a reproductive advantage reflected by a symmetric division rate that is $k_{\text{reproductive}}$ times faster than that of a normal cell, which could correspond to an increased crypt fission rate, as observed in crypts with inactivated *APC* (36, 37). Mutants may also have a survival advantage that confers a longer lifetime than that of wild-type cells by having a death rate that is k_{survival} times the wild-type death rate (λ). This factor can be interpreted as either a longer intrinsic lifespan or a resistance to an ambient chronic cytotoxic event, such as the resistance *p53* inactivation confers against UVB damage or hypoxia (8, 15).

Exponential Growth Model. A stochastic birth process was implemented to model the size distributions of clones that grow exponentially at rate α (38). The probability that a clone at time t contains z cells is:

$$p_z(t) = -\frac{1}{\log[1-p(t)]}\frac{p(t)^z}{z}, \qquad [4]$$

where $p(t) = 1 - \exp(-\alpha t)$. The initiation (mutation) rate does not need to be set because we are concerned only with the size distribution of clones and not their number. For each comparison with the mouse data, we drew 1,000 values from p_z.

Statistical Analysis. A Smirnov two-sample test adapted for discrete data was used to test whether clone-size data from different models were consistent with a single underlying distribution (19). Other statistical analyses were conducted in the R statistical computing language version 2.6.2 (39). Linear least-squares regression was used to fit the simulated mutant-clone perimeter and area growth over time to linear and quadratic functions.

The probability that a mutant will colonize an adjacent empty site depends on the number of mutant and normal neighbors of that site, which is summarized in Table 1. For a mutant with the same replication rate as the normal cells (i.e., the survival mutant), the probability that it will colonize an empty site is equal to the proportion of the empty site's neighbors that are mutants. Thus, the probabilities that it can colonize an empty site with one, two, . . . , or six mutant neighbors (with a total of six neighbors) are 1/6 . . . 6/6. The reproductive mutant replicates 10 times faster than normal and therefore has a higher probability of colonizing empty sites. The empty space will be colonized by the mutant if any mutant neighbor's replication time [drawn from the exponential distribution $E(t;10r)$] is shorter than all of the normal neighbors' times [drawn from $E(t;r)$]. Drawing a random value from $E(t;10r)$ is equivalent to drawing 10 values from $E(t;r)$ and choosing the minimum. In other words, competing with 1 mutant neighbor having a reproductive advantage is equivalent to competing with 10 mutant neighbors lacking the advantage. Therefore, if an empty site has x mutant neighbors and y normal neighbors, the probability that the mutant will colonize the space is

$10x/(10x + y)$, and the probabilities of mutant colonization for a site with one . . . six mutant neighbors are $10/(10 + 5)$ . . . $10 \times 6/(10 \times 6 + 0)$.

Characterization of *p53*-Mutant Clones in Mouse Dorsal Epidermis. Experimental data used for comparison to the exponential and frontier models was drawn from a previously published study (9). Briefly, mice had been exposed to UVB (1,250 J/m^2) for 3, 5, 8, and 10 weeks before being killed, and epidermal sheets from dorsal skin were prepared and then stained with rabbit polyclonal antibody CM-5 for wild-type or mutant murine p53 protein (Novocastra). The sizes of clones were determined by counting the number of adjacent positive nuclei. Clonality of some of these clusters was tested by DNA sequencing. The EPUs were inferred to consist of 16 cells, so we estimated the number of *p53*-mutant EPUs to be the number of p53 positive cells divided by 16. Because clusters of one or two cells were not counted, we did not estimate the number of clones consisting of only one EPU.

ACKNOWLEDGMENTS. This work was supported by National Institutes of Health Grants R01 CA119224 (to D.L.C., C.C.M., and E.G.L.), T32 CA80416 and P01 CA91955 (to D.L.C.), and R01 CA78735 and R01 CA55737 (to D.E.B.) and grants from the Ryan Hill Foundation (to D.L.C.), the Commonwealth Universal Research Enhancement Program of the Pennsylvania Department of Health (to C.C.M.), and the Pew Charitable Trust (to C.C.M.).

1. Jonason AS, *et al.* (1996) Frequent clones of p53-mutated keratinocytes in normal human skin. *Proc Natl Acad Sci USA* 93:14025–14029.
2. Ren ZP, *et al.* (1996) Human epidermal cancer and accompanying precursors have identical p53 mutations different from p53 mutations in adjacent areas of clonally expanded non-neoplastic keratinocytes. *Oncogene* 12:765–773.
3. Califano J, *et al.* (1996) Genetic progression model for head and neck cancer: Implications for field cancerization. *Cancer Res* 56:2488–2492.
4. Franklin WA, *et al.* (1997) Widely dispersed *p53* mutation in respiratory epithelium: A novel mechanism for field carcinogenesis. *J Clin Invest* 100:2133–2137.
5. Czerniak B, *et al.* (1999) Superimposed histologic and genetic mapping of chromosome 9 in progression of human urinary bladder neoplasia: Implications for a genetic model of multistep urothelial carcinogenesis and early detection of urinary bladder cancer. *Oncogene* 18:1185–1196.
6. Galipeau PC, Prevo LJ, Sanchez CA, Longton GM, Reid BJ (1999) Clonal expansion and loss of heterozygosity at chromosomes 9p and 17p in premalignant esophageal (Barrett's) tissue. *J Natl Cancer Inst* 91:2087–2095.
7. Rubin H (2006) What keeps cells in tissues behaving normally in the face of myriad mutations? *Bioessays* 28:515–524.
8. Graeber TG, *et al.* (1996) Hypoxia-mediated selection of cells with diminished apoptotic potential in solid tumours. *Nature* 379:88–91.
9. Zhang W, Remenyik E, Zelterman D, Brash DE, Wikonkal NM (2001) Escaping the stem cell compartment: Sustained UVB exposure allows p53-mutant keratinocytes to colonize adjacent epidermal proliferating units without incurring additional mutations. *Proc Natl Acad Sci USA* 98:13948–13953.
10. Mudgil AV, *et al.* (2003) Ultraviolet B irradiation induces expansion of intraepithelial tumor cells in a tissue model of early cancer progression. *J Invest Dermatol* 121:191–197.
11. Potten CS (1974) The epidermal proliferative unit: The possible role of the central basal cell. *Cell Tissue Kinet* 7:77–88.
12. Clayton E, *et al.* (2007) A single type of progenitor cell maintains normal epidermis. *Nature* 446:185–189.
13. Jones P, Simons BD (2008) Epidermal homeostasis: Do committed progenitors work while stem cells sleep? *Nat Rev Mol Cell Biol* 9:82–88.
14. Klein AM, Doupé DP, Jones PH, Simons BD (2007) Kinetics of cell division in epidermal maintenance. *Phys Rev E Stat Nonlin Soft Matter Phys* 76(2 Pt 1):021910.
15. Ziegler A, *et al.* (1994) Sunburn and p53 in the onset of skin cancer. *Nature* 372:773–776.
16. Zhang W, *et al.* (2005) UVB-induced apoptosis drives clonal expansion during skin tumor development. *Carcinogenesis* 26:249–257.
17. Brash DE, *et al.* (1991) A role for sunlight in skin cancer: UV-induced p53 mutations in squamous cell carcinoma. *Proc Natl Acad Sci USA* 88:10124–10128.
18. Rebel H, *et al.* (2001) Early p53-positive foci as indicators of tumor risk in ultraviolet-exposed hairless mice: Kinetics of induction, effects of DNA repair deficiency, and p53 heterozygosity. *Cancer Res* 61:977–983.
19. Nikiforov AM (1994) Algorithm AS 288: Exact Smirnov two-sample tests for arbitrary distributions. *Appl Stat* 43:265–270.
20. Wilk MB, Gnanadesikan R (1968) Probability plotting methods for the analysis of data. *Biometrika* 55:1–17.
21. Luebeck EG, Heidenreich WF, Hazelton WD, Paretzke HG, Moolgavkar SH (1999) Biologically based analysis of the data for the Colorado uranium miners cohort: Age, dose and dose-rate effects. *Radiat Res* 152:339–351.
22. Eden M (1961) A two dimensional growth process. *Proceedings of the Fourth Berkeley Symposium on Mathematical Statistics and Probability*, ed Neyman J (Univ of California Press, Berkeley), pp 223–239.
23. Folkman J, Hochberg M (1973) Self-regulation of growth in three dimensions. *J Exp Med* 138:745–753.
24. Norton L, Simon R, Brereton HD, Bogden AE (1976) Predicting the course of Gompertzian growth. *Nature* 264:542–545.
25. Cotsarelis G, Sun TT, Lavker RM (1990) Label-retaining cells reside in the bulge area of pilosebaceous unit: Implications for follicular stem cells, hair cycle, and skin carcinogenesis. *Cell* 61:1329–1337.
26. Levy V, Lindon C, Harfe BD, Morgan BA (2005) Distinct stem cell populations regenerate the follicle and interfollicular epidermis. *Dev Cell* 9:855–861.
27. Ito M, *et al.* (2005) Stem cells in the hair follicle bulge contribute to wound repair but not to homeostasis of the epidermis. *Nat Med* 11:1351–1354.
28. Brú A, Albertos S, Subiza LJ, Garcia-Asenjo JL, Brú I (2003) The universal dynamics of tumor growth. *Biophys J* 85:2948–2961.
29. Kai T, Spradling A (2003) An empty *Drosophila* stem cell niche reactivates the proliferation of ectopic cells. *Proc Natl Acad Sci USA* 100:4633–4638.
30. Brawley C, Matunis E (2004) Regeneration of male germline stem cells by spermatogonial dedifferentiation *in vivo*. *Science* 304:1331–1334.
31. McGregor WG, Chen RH, Lukash L, Maher VM, McCormick JJ (1991) Cell cycle-dependent strand bias for UV-induced mutations in the transcribed strand of excision repair-proficient human fibroblasts but not in repair-deficient cells. *Mol Cell Biol* 11:1927–1934.
32. Potten CS, *et al.* (1985) Cell kinetic studies in the epidermis of mouse. III. The percent labelled mitosis (PLM) technique. *Cell Tissue Kinet* 18:59–70.
33. Bursch W, Paffe S, Putz B, Barthel G, Schulte-Hermann R (1990) Determination of the length of the histological stages of apoptosis in normal liver and in altered hepatic foci of rats. *Carcinogenesis* 11:847–853.
34. Potten CS (1996) What is an apoptotic index measuring? A commentary. *Br J Cancer* 74:1743–1748.
35. Goldstein JC, Kluck RM, Green DR (2000) A single cell analysis of apoptosis. Ordering the apoptotic phenotype. *Ann N Y Acad Sci* 926:132–141.
36. Bjerknes M, Cheng H, Hay K, Gallinger S (1997) APC mutation and the crypt cycle in murine and human intestine. *Am J Pathol* 150:833–839.
37. Wasan HS, *et al.* (1998) APC in the regulation of intestinal crypt fission. *J Pathol* 185:246–255.
38. Moolgavkar SH, Luebeck EG, de Gunst MCM, Port RE, Schwarz M (1990) Quantitative analysis of enzyme-altered foci in rat hepatocarcinogenesis experiments–I. Single agent regimen. *Carcinogenesis* 11:1271–1278.
39. R Development Core Team (2008) *R: A Language and Environment for Statistical Computing*. (R Foundation for Statistical Computing, Vienna).
40. Bijwaard H, Brugmans MJP, Schöllnberger H (2006) Can promotion of initiated cells be explained by excess replacement of radiation-inactivated cells? *Radiat Res* 165:741–744.
41. Lu Y-P, Lou Y-R, Peng Q-Y, Xie J-G, Conney AH (2004) Stimulatory effect of topical application of caffeine on UVB-induced apoptosis in the epidermis of p53 and Bax knockout mice. *Cancer Res* 64:5020–5027.